

MFL-Net: An Efficient Lightweight Multi-Scale Feature Learning CNN for COVID-19 Diagnosis From CT Images

Amogh Manoj Joshi¹ and Deepak Ranjan Nayak², *Member, IEEE*

Abstract—Timely and accurate diagnosis of coronavirus disease 2019 (COVID-19) is crucial in curbing its spread. Slow testing results of reverse transcription-polymerase chain reaction (RT-PCR) and a shortage of test kits have led to consider chest computed tomography (CT) as an alternative screening and diagnostic tool. Many deep learning methods, especially convolutional neural networks (CNNs), have been developed to detect COVID-19 cases from chest CT scans. Most of these models demand a vast number of parameters which often suffer from overfitting in the presence of limited training data. Moreover, the linearly stacked single-branched architecture based models hamper the extraction of multi-scale features, reducing the detection performance. In this paper, to handle these issues, we propose an extremely lightweight CNN with multi-scale feature learning blocks called as MFL-Net. The MFL-Net comprises a sequence of MFL blocks that combines multiple convolutional layers with 3×3 filters and residual connections effectively, thereby extracting multi-scale features at different levels and preserving them throughout the block. The model has only 0.78M parameters and requires low computational cost and memory space compared to many ImageNet pretrained CNN architectures. Comprehensive experiments are carried out using two publicly available COVID-19 CT imaging datasets. The results demonstrate that the proposed model achieves higher performance than pretrained CNN models and state-of-the-art methods on both datasets with limited training data despite having an extremely lightweight architecture. The proposed method proves to be an effective aid for the healthcare system in the accurate and timely diagnosis of COVID-19.

Index Terms—Chest CT Scan, COVID-19, deep learning, lightweight CNN, multi-scale feature learning.

Manuscript received 4 October 2021; revised 14 May 2022 and 26 June 2022; accepted 14 July 2022. Date of publication 18 August 2022; date of current version 7 November 2022. This work was supported by the Science and Engineering Research Board (SERB), Department of Science and Technology, Government of India under Project SRG/2020/001460. (Corresponding author: Deepak Ranjan Nayak.)

Amogh Manoj Joshi is with the Department of Electronics and Telecommunication Engineering, Vivekanand Education Society's Institute of Technology, Mumbai, Maharashtra 400074, India (e-mail: joshi-amogh9@gmail.com).

Deepak Ranjan Nayak is with the Department of Computer Science and Engineering, Malaviya National Institute of Technology, Jaipur 302017, India (e-mail: drnayak@ieee.org).

The codes and models are available for users at https://github.com/AmoghJ001/MFL_Net.

This article has supplementary downloadable material available at <https://doi.org/10.1109/JBHI.2022.3196489>, provided by the authors.

Digital Object Identifier 10.1109/JBHI.2022.3196489

I. INTRODUCTION

IN NOVEMBER 2019, a cluster of pneumonia cases of unknown etiology were reported in China. Clinical study of the patients revealed that the reason behind the sudden cases was a novel disease, later named as coronavirus disease 2019 (COVID-19) which belonged to the severe acute respiratory syndrome coronavirus 2 (SARS-CoV-2). The outbreak of this virus soon began and it spread across the globe. On 11 March 2020, the COVID-19 was declared a pandemic by World Health Organization (WHO) following its rapid spread [1]. This virus has infected around 517 million people and caused 6.26 million deaths all across the globe (including US 991 k, Brazil 664 k, India 524 k, Russia 377 k, etc). The repetitive outbreaks of the COVID-19 variants in the form of waves indicate its highly mutating nature. Fever, cough, loss of taste and smell, fatigue and muscle aches are some of the major symptoms of this virus. But recently, lot of cases reported where the patients without even experiencing any of these symptoms were tested positive for COVID-19. A rise in such asymptomatic cases has put a heavy strain on the healthcare system worldwide since it is still an ongoing pandemic and a leading cause of death in many countries. Moreover, the healthcare system would be damaged further if exposed suddenly to a new variant of the virus. Hence, a quick and accurate diagnosis is imperative to control the rapid spread of this virus.

The current standard testing procedure is based on reverse transcription-polymerase chain reaction (RT-PCR) which takes around 4–6 hours to provide results and hence, is quite slow and inefficient [2], [3]. The shortage of RT-PCR test kits also proves to be a major concern for timely detection of the virus and curbing its spread. Hence, clinicians have focused their attention on computed tomography (CT) scans as an alternative and efficient testing method because of their capability in showing clear radiological findings of COVID-19 patients at a fast speed and easy accessibility [2], [4]. Also, CT scans distinctly manifest a blend of multifocal peripheral lung changes of ground-glass opacity (GGO) and consolidation which effectively highlight COVID-19 infections in lungs, even at an early stage which helps in timely detection of the virus [5], [6]. However, the medical experts and radiologists require time in examining and analyzing the CT scans manually and may suffer from fatigue due to the burden of examining patients at a large scale. Thus, an automated system that can accurately analyze CT scans and classify them

quickly as COVID-19 positive or negative is highly needed to tackle the current situation and stabilize the healthcare system in case of further virus outbreaks.

The recent years have witnessed a rise in deep learning (DL) methods, mainly convolutional neural networks (CNNs) for medical image analysis tasks [7]. The COVID-19 pandemic has resulted in numerous studies employing DL methods for predicting COVID-19 infection from chest X-rays and CT scans [1], [6]. CNNs have been proved to be effective in extracting the salient features from chest radiography images. Despite the promising performance of CNNs in some studies, a major issue to be noted is the large quantity of training data that they require to effectively extract the prominent features from the CT images. But, the availability of only a few publicly available datasets makes it harder for the CNN model to learn the accurate features that are required to correctly classify positive COVID-19 samples from negative samples. Also, most of the existing CNN models demand a large number of parameters and more memory space, requiring a considerable inference time while classifying a CT image [5], [8]. Therefore, such heavier models may not be suitable for real-time diagnosis especially in this scenario where obtaining rapid results is highly essential. Although, few lightweight CNN models exist, they do not extract multi-scale features [9], [10] which appears to be very crucial for CT image classification. To address the above issues, in this paper, we present an efficient lightweight CNN with multi-scale feature learning capability which tackles the problem of extracting prominent features even in the presence of limited CT data. Despite having smaller parameters, low memory space and shallow architecture, the proposed CNN model outperforms most of the heavy pretrained CNN models and state-of-the-art approaches. The important contributions of this paper are summarized as follows:

- We propose a very lightweight CNN model (with 0.78 M parameters) coupled with multi-scale feature learning blocks for COVID-19 detection from chest CT scans and term it as MFL-Net.
- The proposed model consists of four multi-scale feature learning (MFL) blocks wherein each block contains a blend of convolutional layers (with only 3×3 and 1×1 filters) and residual connections, which effectively learns feature maps with various size receptive fields (i.e., multi-scale features) and preserves them throughout the block.
- The efficacy of the MFL-Net is verified through an extensive set of experiments on two publicly available COVID-19 CT datasets. Also, we perform mix-dataset evaluation to test the generalization performance of the model. Several ablation studies are performed to find the optimal set of hyperparameters that yield the best results.
- We compare the performance of the proposed MFL-Net with a set of contemporary pretrained CNN models and state-of-the-art methods in terms of classification accuracy, computational cost, and memory.

II. RELATED WORK

Soon after the outbreak of COVID-19, numerous studies were performed to investigate and understand the factors that would help in the diagnosis of COVID-19. Several studies revealed

that chest CT scans manifest clear radiological findings of COVID-19 [1], [2]. Further, studies in [11] and [12] explained the importance and role of artificial intelligence (AI) in screening and diagnosing COVID-19 patients. This further led to a lot of studies for automated diagnosis of COVID-19 from medical images like X-rays and CT Scans. Few machine learning based approaches have developed for COVID-19 diagnosis. For instance, Gaudencio et al. [13] employed a three-dimensional multiscale fuzzy entropy (MFE3D) algorithm with different classifiers for texture-based classification of COVID-19, idiopathic pulmonary fibrosis (IPF) and healthy CT scans, and achieved an accuracy of 89%. Tuncer et al. [14] proposed a fuzzy tree transform-based approach and a multikernel local binary pattern (MKLBP) with cubic SVM to achieve an accuracy of 97.1%. Such machine learning-based methods follow multiple conventional steps (feature extraction, feature selection, and classification) and fall short in extracting the discriminant features, thus paving a solid reason for the application of DL in COVID-19 detection. Xu et al. [15] developed a DL based early-diagnostic system for distinguishing COVID-19 from pneumonia and normal cases with an accuracy of 86.7%. Few similar studies [16], [17], [18], [19], [20] have been made to diagnose COVID from CT scans. He et al. [5] proposed a self supervised transfer learning approach for detecting COVID-19 from CT scans which achieved an accuracy of 86%. Hasan et al. [21] proposed a multi encoder ensemble network named CVR-Net using ResNet50 and Xception as encoders for COVID-19 detection from CT scans. Wang et al. [6] developed a CT scan based DL model called CCSHNet to screen COVID-19 which used two best pretrained CNN models to learn salient features and then fused these features by a discriminant correlation analysis method. Recently, Kaur et al. [8] proposed an automatic method using deep features derived from a MobileNetv2 and a parameter free BAT optimized fuzzy K-nearest neighbor classifier (PF-FKNN) to achieve higher accuracy for COVID-19 diagnosis. Wang et al. [22] proposed a COVID-Net architecture and implemented it with a contrastive cross-site learning strategy to tackle the data heterogeneity across different datasets. In a recent study, Ozyurt et al. [23] proposed a fused dynamic sized exemplars-based pyramid feature generation network (FDEPFGN) and an iterative hybrid feature selector to extract comprehensive features from CT scans. JavadiMoghaddam et al. [24] proposed a CNN model incorporating squeeze excitation (SE) block and Mish activation function for COVID-19 detection from CT scans, while Madan et al. [25] employed a triplet network using few-shot learning to detect COVID-19 with limited CT scans. Besides, DL-based methods have gained popularity for segmenting lesions in COVID-19 CT images as it is crucial for accurate diagnosis and follow-up. Wang et al. [26] proposed a COVID-19 pneumonia lesion segmentation network (COPLNet) that deals with lesions of various scales. Paluru et al. [27] designed a lightweight CNN (Anam-Net) using anamorphic depth embedding to segment anomalies in COVID-19 CT scans. Recently, Wu et al. [28] proposed SRGNet, a sequential region generation network for joint detection and segmentation of COVID-19 lesions in CT scans.

Selecting an appropriate feature extractor and classifier in ML-based approaches has still remained a challenging problem.

On the other hand, most DL-based studies either used heavy CNN models (with large model sizes) or pretrained models with transfer learning which are computationally expensive and need ample memory space. Further, many of them did not focus on learning multi-scale features, which are essential for effectively capturing the minute details of COVID-19 lesions. To handle these problems, Polsinelli et al. [29] built a lightweight CNN model which achieved a test accuracy of 83%. However, this model may not meet the real-time requirements of COVID-19 diagnosis. Thus, a lightweight CNN that could effectively learn prominent features from the limited training data is highly in demand. Another issue that many studies face is validating CNN models using limited training data, which significantly influences the model’s performance. Hence, in this study, we aim to design a lightweight CNN model that learns multi-scale features from the limited chest CT images.

III. DATASET

To perform a comprehensive evaluation of the proposed MFL-Net, we use two COVID-19 CT datasets: COVID-CT and SARS-CoV-2 CT-Scan.

A. COVID-CT Dataset

This dataset [5] from UCSD Research Group contains 349 CT scan images of COVID-19 positive cases and 397 CT scans of COVID-19 negative cases. The positive COVID-19 samples were collected from 143 patients, whereas the Non-COVID samples were collectively obtained from PubMed Central (PMC) and MedPix. The negative cases include CT scans from healthy subjects as well as patients with other type of lung diseases. The images varied in height and width from 153 to 1853 and 124 to 1485, respectively, and were hence resized to 224×224 . The sample images of two classes from this dataset are shown in Fig. S1 in the supplementary information (SI). This dataset was already available in train, validation and test sets. It is worth noting that the data splitting was done based on the patients to ensure no information leakage into validation and test set.

B. SARS-CoV-2 CT-Scan Dataset

For further analyzing the effectiveness of our proposed model, we use another dataset which is comparatively larger than COVID-CT dataset. The SARS-CoV-2 CT-Scan dataset [30] contains 1252 CT scans from 60 COVID-19 positive patients and 1229 CT scans from 60 patients non-infected by COVID-19, but have other pulmonary diseases. In this dataset, the images are varied in height and width from 104 to 484 and 153 to 416, respectively. All the images were therefore resized to 224×224 . Few sample CT images of COVID-19 positive and negative cases are shown in Fig. S2 (SI). Unlike COVID-CT dataset, this dataset was not available in train-test split sets. However, in the base paper [30], the authors adopted 80:20 train-test split ratio without providing any indication of whether data splitting was done based on subjects or not. Therefore, to ensure a fair comparison, we adopted the same data split in our experiments. We further divided the train set into train and validation sets

TABLE I
DESCRIPTION OF COVID-CT AND SARS-CoV-2 CT-SCAN DATASETS

Set	COVID-CT Dataset		SARS-CoV-2 CT-Scan Dataset	
	COVID-19	Non-COVID-19	COVID-19	Non-COVID-19
Train	191	234	802	787
Val	60	58	200	196
Test	98	105	250	246
Total	349	397	1252	1229

in 80:20 ratio, respectively. Table I summarizes the number of images in each set of the COVID-CT and SARS-CoV-2 CT-Scan datasets.

C. Data Augmentation

Medical imaging datasets often encounter a small-size dataset (SSD) problem as data acquisition and medical image annotation are difficult and costly. Less number of training samples hampers the feature extraction of CNN models and thus result in low performance. Augmenting the data is an effective way to tackle this problem. Therefore, we augment each image in the training set using four transformations: (a) Gaussian noise (with mean and standard deviation 0 and 0.01, respectively), (b) horizontal flip, (c) anticlockwise rotation (angle 5°), and (d) clockwise rotation (angle 5°). The details of these operations and the dataset arrangement after augmentation can be found in the supplementary information.

IV. PROPOSED METHODOLOGY

The impetus behind the design of a highly lightweight multi-scale CNN model was to extract multi-scale features from limited CT images, resulting in an efficient COVID-19 detection while preserving the small model size. This section discusses the proposed MFL-Net model in detail. More explanation on the importance of lightweight architecture and multi-scale feature learning can be found in the supplementary information.

A. Proposed MFL-Net

The proposed MFL-Net mainly comprises four multi-scale feature learning (MFL) blocks in its architecture as shown in Fig. 1. The architecture of the proposed model and its various blocks are explained in detail below.

1) *Mini Block*: The MFL block incorporates several three-layered mini blocks denoted as β_{mini} which has a sequence of convolutional (CONV), batch normalization (BN), and ReLU layer. The CONV layer uses a filter of size 3×3 to capture the detailed features at finer levels from the CT images. In this, the padding value has been kept “same” for maintaining a similar feature map size throughout the MFL block. The BN layer prevents the model from overfitting and boosts the learning process, thereby improving the training convergence. The ReLU activation layer is added to introduce non-linearity in the network’s learning process.

Let $\beta_{mini}^N(I)$ represent the output of a mini block with N filters, $\varphi^{f,f,N}(I)$ represent convolution operation with N number of kernels of size $f \times f$, η denote the BN function, and α denote the ReLU activation function. The functioning of the mini block

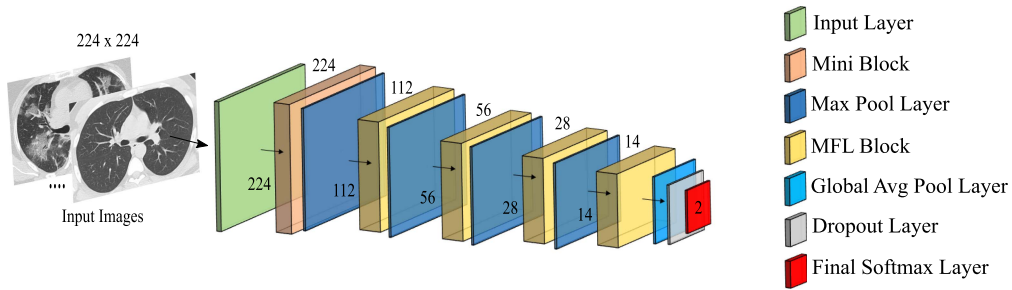


Fig. 1. The overall architecture of the proposed MFL-Net. It consists of four MFL blocks; each follows a max-pool layer. The output of the last MFL block is fed to a global average pooling (GAP) layer and a classification layer to classify each input image as COVID-19 or Non-COVID-19.

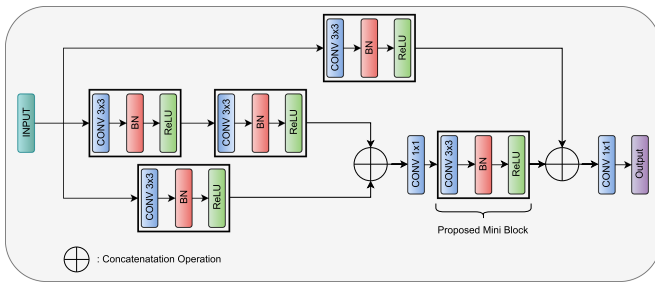


Fig. 2. Detailed illustration of the proposed multi-scale feature learning (MFL) block. It consists of five convolutional layers with 3×3 filters and residual connections to capture features with various sizes receptive fields (i.e., multi-scale features). The 1×1 convolutional layers are used to reduce the number of channels in the feature maps.

β_{mini}^N can be expressed mathematically as follows

$$\beta_{mini}^N(I) = \alpha(\eta(\varphi^{3,3,N}(I))) \quad (1)$$

2) **MFL Block:** The mini blocks are used at several stages throughout the MFL block. The MFL block is a multi-scale feature extraction module as shown in Fig. 2 which is repeated four times throughout the proposed MFL-Net architecture. The purpose of multi-scale feature extraction is to enable the model to learn features of different receptive field sizes using a set of filters and enhance its learning process, improving its generalization performance on unseen images. The small size filters like 3×3 help in extracting the detailed features like patchy shadows, small patches, and GGO, which are found in the radiographic scans of COVID-19 positive patients. In contrast, the large size filters such as 5×5 and 7×7 help to learn the coarse features like the shape of the lung region. To learn multi-scale features, i.e., features with varying sizes of receptive fields, filters of various sizes such as 3×3 , 5×5 and 7×7 are generally applied in parallel over the input data followed by the concatenation of extracted feature maps [9], [10]. However, large size filters require more number of parameters compared to small size filters. Specifically, a CONV layer with 5×5 kernel size takes more than double the parameters taken by a CONV layer of the same number of filters with 3×3 kernel size, whereas a CONV layer with 7×7 kernel size takes more than five times the parameters taken by a CONV layer with 3×3 kernel size. Hence, to maintain a lightweight architecture, we used multiple CONV layers with 3×3 kernel size in an effective way to capture

the same features of a 5×5 and 7×7 kernel. In particular, two CONV layers with 3×3 filter size can be used sequentially to extract features with a receptive field size of 5. The related equations to compute the size of the receptive field can be found in the supplementary information.

Similarly, three CONV layers with a kernel size of 3×3 can be used sequentially to extract features with a receptive field of size 7. Hence, using multiple CONV layers with only 3×3 kernel size reduces the parameters drastically than using a single CONV layer with 5×5 or 7×7 kernel size. Inspired by this, the proposed MFL-Net combines a set of 3×3 filters and residual connections in an effective way to capture features with a receptive field of size 7 while maintaining minimal parameters.

In the MFL block, the input is first passed through two parallel streams with a single mini block in one stream and two mini blocks stacked one after another in the second stream, which extracts features with receptive field size 5. The features from both the streams are fused using concatenation which ensures the features have receptive fields of size 3 and 5 and are passed to a CONV layer with 1×1 kernel size, which reduces the number of channels in the feature maps from $n \times n \times f$ to $n \times n \times (f/2)$. The output of this layer is then fed to another mini-block to enlarge the size of the receptive fields. In particular, this mini block extracts features with receptive field size 5 and 7. The output of this mini block is concatenated again with the input of the MFL block passed through another mini block via a residual skip connection to ensure multi-scale feature extraction as it extracts features with receptive field size 3, 5, and 7. The output of this concatenation is further passed to a CONV layer with 1×1 kernel size for channel reduction in the output feature maps.

Let $\beta_{MFL}^N(I)$ denote the output of MFL block on input I with N filters and \oplus denote concatenation operation. The functioning of MFL block can be mathematically stated as

$$\beta' = \beta_{mini}^N(\beta_{mini}^N(I)) \oplus \beta_{mini}^N(I) \quad (2)$$

$$\beta_{MFL}^N(I) = \varphi^{1,1,N}(\beta_{mini}^N(\varphi^{1,1,N}(\beta'))) \oplus \beta_{mini}^N(I) \quad (3)$$

Thus, the output of the MFL block contains a perfect amalgamation of multi-scale features using only 3×3 filters while preserving a lightweight architecture.

3) **Overall MFL-Net Architecture:** As shown in Fig. 1, the input image is first passed through a mini block which initiates the feature learning process and is then fed to a max-pooling layer with kernel size 2×2 to reduce the feature map size.

TABLE II
MFL-NET ARCHITECTURE SUMMARY

Layers	Description	Output Size
Mini Block	$[3 \times 3 \text{ conv}] \times 1$	$224 \times 224 \times 16$
Pooling	$2 \times 2 \text{ max pool}, s = 2$	$112 \times 112 \times 16$
MFL Block (1)	$[1 \times 1 \text{ conv}] \times 2$ $[3 \times 3 \text{ conv}] \times 5$	$112 \times 112 \times 16$
Pooling	$2 \times 2 \text{ max pool}, s = 2$	$56 \times 56 \times 16$
MFL Block (2)	$[1 \times 1 \text{ conv}] \times 2$ $[3 \times 3 \text{ conv}] \times 5$	$56 \times 56 \times 32$
Pooling	$2 \times 2 \text{ max pool}, s = 2$	$28 \times 28 \times 32$
MFL Block (3)	$[1 \times 1 \text{ conv}] \times 2$ $[3 \times 3 \text{ conv}] \times 5$	$28 \times 28 \times 64$
Pooling	$2 \times 2 \text{ max pool}, s = 2$	$14 \times 14 \times 64$
MFL Block (4)	$[1 \times 1 \text{ conv}] \times 2$ $[3 \times 3 \text{ conv}] \times 5$	$14 \times 14 \times 128$
Global Average Pool		$1 \times 1 \times 128$
Final Classification Layer	2-d fc (dropout 0.5), Softmax	$1 \times 1 \times 2$

The model then includes four MFL blocks sequentially which enable efficient multi-scale feature extraction, each followed by a max-pooling layer for subsequent feature map size reduction. The output of the last MFL block is passed to a global average pooling (GAP) layer, which follows a dropout layer with a value of 0.5. A classification layer of two neurons is introduced at the end with softmax activation for classifying the CT images as COVID-19 or Non-COVID-19. In a nutshell, the MFL-Net is a highly lightweight model with merely 0.78 million parameters and a multi-scale feature learning architecture, which accounts for its superior performance in distinguishing COVID-19 positive samples from the negative ones. Table II shows the network configuration of the proposed MFL-Net.

V. EXPERIMENTS AND RESULTS

In this section, we present the implementation details, performance evaluation metrics and the experimental results of the proposed MFL-Net model on both the datasets. To further evaluate the efficacy of the proposed model, we compare its results with ImageNet pretrained models along with the existing methods. Also, we perform ablation studies to analyze the effect of various influencing factors like activation functions [31], weight initialization techniques [32], [33], and pooling methods. The results of ablation studies are presented in Tables S2–S4 (SI).

A. Implementation Details

The proposed MFL-Net was validated on two datasets: COVID-CT dataset and SARS-CoV-2 CT-Scan dataset. To prevent overfitting and provide good generalization, we augmented the train set of both datasets using several transformations such as Gaussian noise, horizontal flip, and both clockwise and anticlockwise rotations. There were two neurons with softmax activation in the final classification layer, and the loss function was chosen as categorical cross-entropy. The mini-batch size and number of epochs were set to 32 and 70, respectively. A different initial learning rate was chosen for the two datasets, decayed by a factor of 0.5 if the validation performance does not improve within four epochs. Since the COVID-19 CT dataset

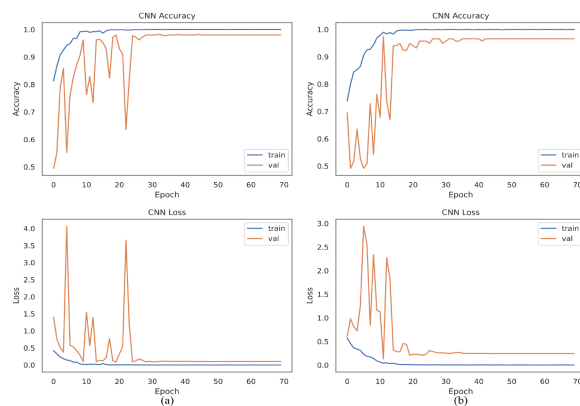


Fig. 3. Training curves on both datasets (top: accuracy vs. epoch, bottom: loss vs. epoch): (a) COVID-CT and (b) SARS-CoV-2 CT-Scan.

TABLE III
CLASSIFICATION RESULTS (IN %) OF PROPOSED MODEL ON COVID-CT AND SARS-CoV-2 CT-SCAN DATASET

Dataset	Acc	F1	AUC	Spec	Sens	Prec
COVID-CT	93.59	94.06	93.43	98.10	88.78	97.75
SARS-CoV-2 CT-Scan	98.79	98.78	98.79	98.78	98.80	98.80

has fewer images, a slow initial learning rate of 0.0001 was chosen, whereas, for the SARS-CoV-2 CT-Scan dataset, a relatively faster learning rate of 0.001 was chosen, which led to an improvement in detection performance. For experiments on both datasets, Xavier weight initializer was used. All experiments were implemented using Keras framework with Tensorflow as backend. It is worth noting that intensity normalization has been applied over all images as a preprocessing step to preserve the numerical stability in the network.

To evaluate the proposed MFL-Net as well as other existing models, we used different evaluation metrics such as accuracy (Acc), F1-score, specificity (Spec), sensitivity (Sen), precision (Prec), and area-under-the-curve (AUC).

B. Evaluation of Proposed Model

Since both datasets contained samples of different patients, the proposed model was trained and tested on these datasets separately to better understand its effectiveness and learning capability. The results on both datasets are explained in detail below.

The training curves obtained by our MFL-Net on both datasets are shown in Fig. 3. It can be seen that the model is converged well within 70 epochs. The model achieved an accuracy of 93.59% and 98.79% on COVID-CT and SARS-CoV-2 CT-Scan dataset, respectively. Table III lists the detailed classification results on both the datasets. Fig. 4 shows the confusion matrices obtained by our MFL-Net on the test set of both datasets. It can be observed that on COVID-CT dataset, only two samples were wrongly classified as COVID-19 positive among 105 COVID-19 negative samples, and 11 among 98 COVID-19 positive samples were misclassified as COVID-19 negative. While on SARS-CoV-2 CT-Scan dataset, only three samples were wrongly classified as COVID-19 negative and positive. The better performance

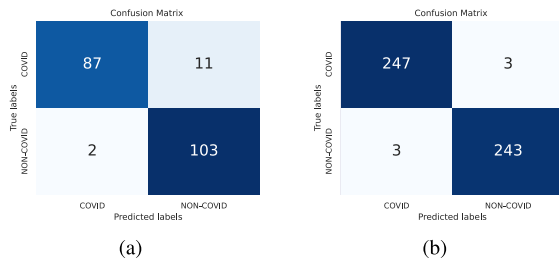


Fig. 4. Confusion matrix obtained by MFL-Net on (a) COVID-CT and (b) SARS-CoV-2 CT-Scan dataset.

TABLE IV
RESULTS OF MIX-DATASET ANALYSIS

Model	Acc	F1	AUC
VGG-16	93.79	93.85	93.81
DenseNet-121	95.64	95.68	95.63
ResNet-50	94.53	94.54	94.53
InceptionV3	94.10	94.25	94.02
Xception	94.53	94.54	94.53
EfficientNetB0	95.64	95.68	95.63
MobileNet-V2	95.35	95.39	95.35
Our MFL-Net	96.13	96.22	96.12

on this dataset can be majorly attributed to the larger number of training samples. It is worth noting here that we achieved the best results with the swish activation function instead of ReLU in the MFL block on SARS-CoV-2 CT-Scan dataset.

1) *Mixed-Dataset Evaluation*: Along with intra-dataset experiments, we also performed a comprehensive mix-dataset evaluation by combining the images of both datasets used. In this experiment, we built the train, validation, and test sets by selecting images from both datasets in the same split ratio. The objective of this experiment was to allow the model to learn from samples of both datasets, increasing diversity in training data. This situation is closer to a real-time scenario. We also evaluated the performance of several ImageNet pretrained models under the same experimental settings. Table IV shows a performance comparison of MFL-Net with ImageNet models. It can be seen that our MFL-Net outperformed the ImageNet models with an accuracy of 96.13%, indicating its good generalization capability. It is worth noting that the same four augmentation techniques discussed earlier in this paper have been adopted in this experiment.

C. Comparison With GAN-Based Augmentation

Generative adversarial networks (GANs) have recently been used for augmenting data in a wide range of medical image analysis tasks where training data is limited [34], [35]. Along with classic data augmentation (CDA) as discussed in Section V-A, we employed a deep convolutional GAN (DCGAN) for generating synthetic CT images, which can be used for data augmentation. The architecture of DCGAN consists of a generator and a discriminator model, which was inspired from [35]; however, it has a few additional upsampling and downsampling layers. Finally, we trained the MFL-Net using the train set combined with GAN-generated images and compared the performance

TABLE V
PERFORMANCE COMPARISON WITH GAN-BASED AUGMENTATION

Method	COVID-CT Dataset			SARS-COV-2 Dataset		
	Acc	F1	AUC	Acc	F1	AUC
CDA	93.59	94.06	93.43	98.79	98.78	98.79
GAN	92.61	92.84	92.58	97.78	97.79	97.79

TABLE VI
COMPARISON OF MODEL PARAMETERS AND SIZES

Model	Parameter (M)	Size (MB)
VGG-16	134.26	512.27
ResNet-50	23.53	90.48
Inception V3	21.77	84
Xception	20.81	79.97
DenseNet-121	6.95	27.94
MobileNet V2	2.26	9.51
EfficientNet B0	4.05	16.84
Our MFL-Net	0.78	3.22

with CDA as shown in Table V. It can be noticed that both the augmentation approaches achieved comparable results, but CDA achieved a slightly higher accuracy on both datasets. However, in the future, we aim to explore the advanced GAN architectures for improved classification results. It is noteworthy that the number of augmented images in both approaches was kept similar for fair comparisons.

D. Comparison With Imagenet Pretrained Models

To demonstrate the efficacy of our MFL-Net, we also investigated the performance of ImageNet pretrained CNN architectures by fine-tuning them on separate CT scan datasets used in our experiments and compared their results with that of our model. The pretrained models include VGG-16 [36], ResNet-50 [37], DenseNet-121 [38], MobileNet V2 [39], EfficientNet B0 [40], Inception V3 [41], and Xception [42]. Initially, a comparison was made on model size, specifically in the context of model parameters in millions and memory space required in megabytes (MB) as listed in Table VI.

It can be seen that most ImageNet pretrained models are extremely heavy like VGG-16 with 134.26 M, ResNet-50 with 23.5 M parameters, Inception V3 with 21.77 M parameters and DenseNet-121 with 6.95 M parameters as compared to our proposed model which requires only 0.78 M parameters (about 0.58% of VGG-16, 3.31% of ResNet-50, 3.58% of Inception V3 and 11.22% of DenseNet-121). It also occupies a less memory space as compared to others and thus, is more suitable for real-time COVID-19 diagnosis using CT images. Tables VII and VIII show the classification results of the ImageNet pretrained CNN architectures and our proposed model on COVID-CT and SARS-CoV-2 CT-Scan datasets, respectively. It can be observed that our model outperformed all the ImageNet models on COVID-CT dataset and achieved comparable or better performance than most models on SARS-CoV-2 CT-Scan dataset.

On COVID-CT dataset, MFL-Net achieved superior performance than all the ImageNet models despite its lighter architecture; whereas, on the SARS-CoV-2 CT-Scan dataset, our MFL-Net outperformed MobileNet V2 and Inception-V3, and achieved similar accuracy as of VGG-16 and ResNet-50.

TABLE VII

PERFORMANCE COMPARISON WITH IMAGENET PRETRAINED CNN MODELS ON COVID-CT DATASET

Model	Acc	F1	AUC	Spec	Sens	Prec
VGG-16	88.17	88.35	88.23	86.67	89.80	86.27
DenseNet-121	92.61	92.95	92.55	94.29	90.82	93.68
ResNet-50	93.10	93.45	93.02	95.24	90.82	94.68
Inception V3	92.11	92.52	92.04	94.29	89.80	93.62
Xception	90.14	90.47	90.13	90.48	89.80	89.80
EfficientNet B0	90.64	90.99	90.61	91.42	89.79	90.72
MobileNet V2	91.62	92.01	91.56	93.33	89.79	92.63
Our MFL-Net	93.59	94.06	93.43	98.10	88.78	97.75

TABLE VIII

PERFORMANCE COMPARISON WITH IMAGENET PRETRAINED CNN MODELS ON SARS-CoV-2-CT-SCAN DATASET

Model	Acc	F1	AUC	Spec	Sens	Prec
VGG-16	98.79	98.78	98.79	99.19	98.40	99.19
DenseNet-121	98.99	98.99	99.00	100	98.00	100
ResNet-50	98.79	98.79	98.80	100	97.60	100
InceptionV3	97.98	98.00	98.00	100	96.00	100
Xception	99.19	99.19	99.20	100	98.40	100
EfficientNet B0	98.99	98.99	99.00	100	98.00	100
MobileNet V2	98.58	98.59	98.59	99.59	97.60	99.59
Our MFL-Net	98.79	98.78	98.79	98.78	98.80	98.80

While Xception is 27 times heavier, it achieved accuracy greater than MFL-Net by only 0.4%. Further, DenseNet-121 (9 times heavier) and EfficientNet B0 (5.2 times heavier) achieved comparable accuracy with our model, which further proved the efficacy of the proposed MFL-Net despite having a very lightweight architecture. To summarize, compared to DenseNet-121 and Inception V3 which learn multi-scale features, our MFL-Net achieved better performance, indicating a better feature learning capability in the presence of limited training data. Further, our model outperformed lightweight models such as MobileNet V2 and EfficientNet B0. It is worth mentioning that all the ImageNet models were implemented under a similar experimental setup for both datasets.

E. Comparison With Existing Methods

Apart from evaluating the performance of the proposed model, we further compared the results of our model with the state-of-the-art COVID-19 diagnosis methods on both datasets separately. A comparison with the existing works that used COVID-CT dataset [5], [8], [16], [18], [21], [29], [43], [44] has been made in Table IX. It can be seen that our MFL-Net outperforms all the existing approaches in terms of classification accuracy and F1-score. It is worth noting that all the existing methods were implemented under a similar experimental setting to derive a fair comparison. It can also be observed that MFL-Net outperforms other multi-scale based CNN methods proposed by Wang et al. [6], He et al. [5], and Hasan et al. [21]. The CRNet [5] obtained the least performance, and this is due to the fact that CRNet followed VGG like linearly stacked architecture and did not extract multi-scale features from the CT images. Also, despite having the lightest architecture among all these state-of-the-art works, our model achieved the best results on this dataset.

TABLE IX

PERFORMANCE COMPARISON WITH EXISTING WORKS ON COVID-CT DATASET

Reference	Method	Acc (%)	F1 (%)
He et al. [5]	CRNet	72.00	76.00
He et al. [5]	DenseNet-169 with Self-Trans	86.00	85.00
Hasan et al. [21]	CVR-Net	78.00	78.00
Polsinelli et al. [29]	SqueezeNet	75.86	76.77
Saqib et al. [18]	ShuffleNet-v2-x1.0	74.38	75.50
Saqib et al. [18]	EfficientNetB4	80.30	81.13
Wang et al. [22]	Redesigned COVID-Net	78.69	78.83
Wang et al. [16]	M-Inception	83.74	83.74
Kaur et al. [8]	MobileNetv2 and PF-FKNN	84.24	83.16
Zhang et al. [44]	7L-CNN	86.69	87.20
Nayak et al. [43]	ResNet-34	86.69	88.00
Sen et al. [48]	CNN + SVM	90.00	88.55
Our model	MFL-Net	93.59	94.06

TABLE X

PERFORMANCE COMPARISON WITH EXISTING WORKS ON SARS-CoV-2 CT-SCAN DATASET

Reference	Method	Acc (%)	F1 (%)
Wang et al. [22]	Redesigned COVID-Net	90.83	90.87
Angelov et al. [30]	XDNN	97.38	97.31
Angelov et al. [30]	VGG-16	94.96	94.97
Foysal et al. [45]	Ensemble CNN	96.00	95.60
Pathak et al. [46]	DBM	97.23	97.89
Pathak et al. [46]	DBM + MADE	98.37	98.14
Kaur et al. [47]	MobileNetv2 + ResNet50	98.35	98.41
Sen et al. [48]	CNN + SVM	98.39	98.00
Kaur et al. [8]	MobileNetv2 and PF-FKNN	99.38	99.20
Our model	MFL-Net	98.79	98.78

Similarly, a comparison with the existing works [8], [22], [45], [46], [47], [48] validated on SARS-CoV-2 CT-Scan dataset [30] has been made in Table X. It can be seen that the proposed model outperforms almost all the existing works. It is worth highlighting that our lightweight approach achieved higher performance than the works which used multiple models and ensemble approaches [46], [47]. Kaur et al. [8] used MobileNet V2 along with FKNN model which is approximately 4.35 times heavier than our model; however, it achieved a slightly higher accuracy. The superior performance of our proposed model on both datasets can be majorly attributed to its multi-scale feature learning capability coupled with its highly lightweight network, thus proving its robustness and efficacy.

F. Grad-CAM Visualization of MFL-Net

The comparison with ImageNet pretrained models and state-of-the-art DL-based approaches demonstrated the effectiveness of our MFL-Net model. However, to get a deeper understanding of the behavior of the proposed model and to understand the features on which the model is focusing, we used Grad-CAM [49] visualizations which provide a visual interpretation of the model predictions. Grad-CAM also helps cross-check whether the model learns the appropriate features from the image instead of the background. Fig. 5 depicts the heatmap results for both COVID-19 and Non-COVID-19 samples of both the datasets using Grad-CAM visualizations. From these heatmaps, it can be seen that in COVID-19 CT scans, our model can accurately locate the infected lung regions, whereas, for Non-COVID-19 CT scans, there is no indication of infected areas. This exhibits

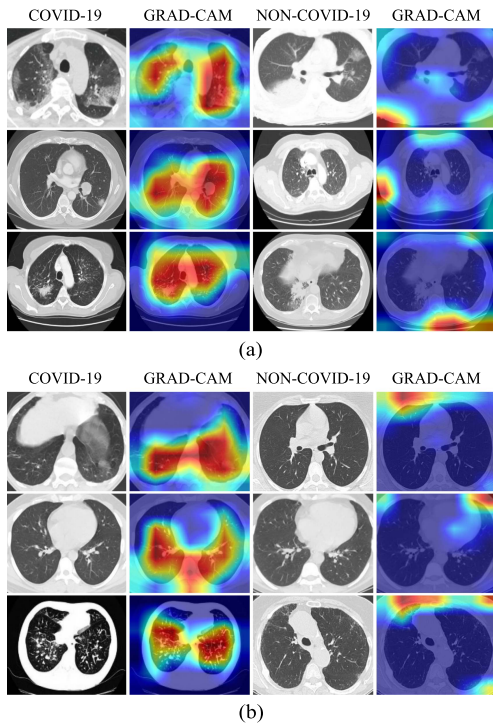


Fig. 5. GradCAM visualization results of MFL-Net on sample images of two classes: COVID-19 and Non-COVID-19 for both datasets: (a) COVID-CT dataset and (b) SARS-CoV-2 CT-Scan dataset.

better interpretability of the classification results by our model and supports the superior classification performance.

G. Limitations

The current study has some limitations. Although our method performs better in the presence of limited data, the size of the datasets considered is reasonably small, with data collected from only a few COVID-19 patients, and the datasets do not contain more diverse CT image data. Furthermore, the datasets do not include patients with different stages of COVID-19 infection and patients with asymptomatic cases. The studies in [50] and [51] have shown the radiological findings in CT scans at different stages of COVID-19 infection. However, there is no such CT image dataset containing different severity levels yet available publicly to verify the effectiveness of the model. Further, it has been observed that there are abnormal findings in CT images of asymptomatic COVID-19 cases [52], [53] and how well the proposed model can perform on such data needs further investigation. In future work, we will verify the effectiveness of the proposed model using a large and diverse COVID-19 CT dataset with data from patients at different severity levels. Also, we will try to evaluate the model on CT images of asymptomatic cases.

VI. CONCLUSION

This paper proposed an extremely lightweight CNN model termed as MFL-Net with multi-scale feature learning capability to detect COVID-19 infection from chest CT scans accurately. The MFL-Net includes a set of MFL blocks that effectively combine multiple convolutional layers and residual connections

to extract multi-scale features. This has resulted in a highly lightweight architecture with only 0.78 M parameters. Extensive experiments on two COVID-19 CT datasets indicated that MFL-Net achieved superior classification performance with fewer model parameters and memory space, making it suitable for real-time COVID-19 diagnosis. In future, the efficacy of the proposed model can be tested on a variety of image classification tasks. Also, we intend to design more effective feature enhancement modules to enhance the COVID-19 detection performance further.

REFERENCES

- [1] F. Shi et al., "Review of artificial intelligence techniques in imaging data acquisition, segmentation and diagnosis for COVID-19," *IEEE Rev. Biomed. Eng.*, vol. 14, pp. 4–15, Apr. 2021.
- [2] D. Dong et al., "The role of imaging in the detection and management of COVID-19: A review," *IEEE Rev. Biomed. Eng.*, vol. 14, pp. 16–29, 2021.
- [3] Y. Fang et al., "Sensitivity of chest CT for COVID-19: Comparison to RT-PCR," *Radiology*, vol. 296, no. 2, pp. E115–E117, 2020.
- [4] X. Li et al., "CT imaging changes of corona virus disease 2019 (COVID-19): A multi-center study in Southwest China," *J. Transl. Med.*, vol. 18, pp. 1–8, 2020.
- [5] X. He et al., "Sample-efficient deep learning for COVID-19 diagnosis based on CT scans," *MedRxiv*, 2020, doi: [10.1101/2020.04.13.20063941](https://doi.org/10.1101/2020.04.13.20063941).
- [6] S.-H. Wang, D. R. Nayak, D. S. Guttery, X. Zhang, and Y.-D. Zhang, "COVID-19 classification by CCSHnet with deep fusion using transfer learning and discriminant correlation analysis," *Inf. Fusion*, vol. 68, pp. 131–148, 2021.
- [7] H.-C. Shin et al., "Deep convolutional neural networks for computer-aided detection: CNN architectures, dataset characteristics and transfer learning," *IEEE Trans. Med. Imag.*, vol. 35, no. 5, pp. 1285–1298, May 2016.
- [8] T. Kaur, T. K. Gandhi, and B. K. Panigrahi, "Automated diagnosis of COVID-19 using deep features and parameter free BAT optimization," *IEEE J. Transl. Eng. Health Med.*, vol. 9, pp. 1–9, 2021.
- [9] S. Li et al., "Multi-instance multi-scale CNN for medical image classification," in *Proc. Int. Conf. Med. Image Comput. Comput. Assist. Intervention*, 2019, pp. 531–539.
- [10] C. Szegedy et al., "Going deeper with convolutions," in *Proc. IEEE Conf. Comput. Vis. Pattern Recognit.*, 2015, pp. 1–9.
- [11] X. Mei et al., "Artificial intelligence-enabled rapid diagnosis of patients with COVID-19," *Nature Med.*, vol. 26, no. 8, pp. 1224–1228, 2020.
- [12] T. T. Nguyen, Q. V. H. Nguyen, D. T. Nguyen, E. B. Hsu, S. Yang, and P. Eklund, "Artificial intelligence in the battle against coronavirus (COVID-19): A survey and future research directions," 2020, *arXiv:2008.07343*.
- [13] A. S. Gaudêncio et al., "Evaluation of COVID-19 chest computed tomography: A texture analysis based on three-dimensional entropy," *Biomed. Signal Process. Control*, vol. 68, 2021, Art. no. 102582.
- [14] T. Tuncer, F. Ozyurt, S. Dogan, and A. Subasi, "A novel COVID-19 and pneumonia classification method based on F-transform," *Chemometrics Intell. Lab. Syst.*, vol. 210, 2021, Art. no. 104256.
- [15] X. Xu et al., "A deep learning system to screen novel coronavirus disease 2019 pneumonia," *Engineering*, vol. 6, no. 10, pp. 1122–1129, 2020.
- [16] S. Wang et al., "A deep learning algorithm using CT images to screen for corona virus disease (COVID-19)," *Eur. Radiol.*, vol. 31, pp. 6096–6104, 2021.
- [17] S. Thakur and A. Kumar, "X-ray and CT-scan-based automated detection and classification of COVID-19 using convolutional neural networks (CNN)," *Biomed. Signal Process. Control*, vol. 69, 2021, Art. no. 102920.
- [18] M. Saqib et al., "COVID-19 detection from radiographs: Is deep learning able to handle the crisis?" *Signals*, vol. 3, pp. 296–312, 2022, doi: [10.3390/signals3020019](https://doi.org/10.3390/signals3020019).
- [19] M. M. Tareh, N. Zhu, T. A. A. Ali, A. S. Hameed, and M. L. Mutar, "Transfer learning to detect COVID-19 automatically from X-ray images using convolutional neural networks," *Int. J. Biomed. Imag.*, vol. 2021, 2021, Art. no. 8828404.
- [20] A. Subasi, A. Mitra, F. Ozyurt, and T. Tuncer, "Automated COVID-19 detection from CT images using deep learning," in *Computer-Aided Design and Diagnosis Methods for Biomedical Applications*. Boca Raton, FL, USA: CRC Press, 2021, pp. 153–176.

- [21] M. Hasan et al., "CVR-Net: A deep convolutional neural network for coronavirus recognition from chest radiography images," 2020, *arXiv:2007.11993*.
- [22] Z. Wang, Q. Liu, and Q. Dou, "Contrastive cross-site learning with redesigned net for COVID-19 CT classification," *IEEE J. Biomed. Health Informat.*, vol. 24, no. 10, pp. 2806–2813, Oct. 2020.
- [23] F. Ozyurt, T. Tuncer, and A. Subasi, "An automated COVID-19 detection based on fused dynamic exemplar pyramid feature extraction and hybrid feature selection using deep learning," *Comput. Biol. Med.*, vol. 132, 2021, Art. no. 104356.
- [24] S. JavadiMoghaddam and H. Gholamalinejad, "A novel deep learning based method for COVID-19 detection from CT image," *Biomed. Signal Process. Control*, vol. 70, 2021, Art. no. 102987.
- [25] S. Madan, S. Chaudhury, and T. K. Gandhi, "Automated detection of COVID-19 on a small dataset of chest CT images using metric learning," in *Proc. Int. Joint Conf. Neural Netw.*, 2021, pp. 1–8.
- [26] G. Wang et al., "A noise-robust framework for automatic segmentation of COVID-19 pneumonia lesions from CT images," *IEEE Trans. Med. Imag.*, vol. 39, no. 8, pp. 2653–2663, Aug. 2020.
- [27] N. Paluru et al., "Anam-Net: Anamorphic depth embedding-based lightweight CNN for segmentation of anomalies in COVID-19 chest CT images," *IEEE Trans. Neural Netw. Learn. Syst.*, vol. 32, no. 3, pp. 932–946, Mar. 2021.
- [28] J. Wu et al., "Joint segmentation and detection of COVID-19 via a sequential region generation network," *Pattern Recognit.*, vol. 118, 2021, Art. no. 108006.
- [29] M. Polsinelli, L. Cinque, and G. Placidi, "A light CNN for detecting COVID-19 from CT scans of the chest," *Pattern Recognit. Lett.*, vol. 140, pp. 95–100, 2020.
- [30] P. Angelov and E. A. Soares, "SARS-CoV-2 CT-scan dataset: A large dataset of real patients CT scans for SARS-CoV-2 identification," *MedRxiv*, 2020, doi: [10.1101/2020.04.24.20078584](https://doi.org/10.1101/2020.04.24.20078584).
- [31] P. Ramachandran, B. Zoph, and Q. Le, "Swish: A self-gated activation function," 2017, *arXiv:1710.05941*.
- [32] X. Glorot and Y. Bengio, "Understanding the difficulty of training deep feedforward neural networks," in *Proc. 13th Int. Conf. Artif. Intell. Statist.*, 2010, pp. 249–256.
- [33] K. He, X. Zhang, S. Ren, and J. Sun, "Delving deep into rectifiers: Surpassing human-level performance on ImageNet classification," in *Proc. IEEE Int. Conf. Comput. Vis.*, 2015, pp. 1026–1034.
- [34] H. Salehinejad, E. Colak, T. Dowdell, J. Barfett, and S. Valaee, "Synthesizing chest X-ray pathology for training deep convolutional neural networks," *IEEE Trans. Med. Imag.*, vol. 38, no. 5, pp. 1197–1206, May 2019.
- [35] M. Frid-Adar, I. Diamant, E. Klang, M. Amitai, J. Goldberger, and H. Greenspan, "GAN-based synthetic medical image augmentation for increased CNN performance in liver lesion classification," *Neurocomputing*, vol. 321, pp. 321–331, 2018.
- [36] S. Liu and W. Deng, "Very deep convolutional neural network based image classification using small training sample size," in *Proc. 3rd IAPR Asian Conf. Pattern Recognit.*, 2015, pp. 730–734.
- [37] K. He, X. Zhang, S. Ren, and J. Sun, "Deep residual learning for image recognition," in *Proc. IEEE Conf. Comput. Vis. Pattern Recognit.*, 2016, pp. 770–778.
- [38] G. Huang, Z. Liu, L. Van Der Maaten, and K. Q. Weinberger, "Densely connected convolutional networks," in *Proc. IEEE Conf. Comput. Vis. Pattern Recognit.*, 2017, pp. 4700–4708.
- [39] M. Sandler, A. Howard, M. Zhu, A. Zhmoginov, and L.-C. Chen, "MobileNetV2: Inverted residuals and linear bottlenecks," in *Proc. IEEE Conf. Comput. Vis. Pattern Recognit.*, 2018, pp. 4510–4520.
- [40] M. Tan and Q. Le, "EfficientNet: Rethinking model scaling for convolutional neural networks," in *Proc. Int. Conf. Mach. Learn.*, 2019, pp. 6105–6114.
- [41] C. Szegedy, V. Vanhoucke, S. Ioffe, J. Shlens, and Z. Wojna, "Rethinking the inception architecture for computer vision," in *Proc. IEEE Conf. Comput. Vis. Pattern Recognit.*, 2016, pp. 2818–2826.
- [42] F. Chollet, "Xception: Deep learning with depthwise separable convolutions," in *Proc. IEEE Conf. Comput. Vis. Pattern Recognit.*, 2017, pp. 1251–1258.
- [43] S. R. Nayak, D. R. Nayak, U. Sinha, V. Arora, and R. B. Pachori, "Application of deep learning techniques for detection of COVID-19 cases using chest X-ray images: A comprehensive study," *Biomed. Signal Process. Control*, vol. 64, 2021, Art. no. 102365.
- [44] Y.-D. Zhang, S. C. Satapathy, L.-Y. Zhu, J. M. Górriz, and S.-H. Wang, "A seven-layer convolutional neural network for chest CT based COVID-19 diagnosis using stochastic pooling," *IEEE Sensors J.*, early access, Sep. 22, 2020, doi: [10.1109/JSEN.2020.3025855](https://doi.org/10.1109/JSEN.2020.3025855).
- [45] M. Foyсал and A. A. Hossain, "COVID-19 detection from chest CT images using ensemble deep convolutional neural network," in *Proc. 2nd Int. Conf. Emerg. Technol.*, 2021, pp. 1–6.
- [46] Y. Pathak, P. K. Shukla, and K. V. Arya, "Deep bidirectional classification model for COVID-19 disease infected patients," *IEEE/ACM Trans. Comput. Biol. Bioinf.*, vol. 18, no. 4, pp. 1234–1241, Jul./Aug. 2021.
- [47] T. Kaur and T. K. Gandhi, "Automated diagnosis of COVID-19 from CT scans based on concatenation of Mobilenetv2 and ResNet50 features," in *Proc. 5th Int. Conf. Comput. Vis. Image Process.*, 2021, pp. 149–160.
- [48] S. Sen, S. Saha, S. Chatterjee, S. Mirjalili, and R. Sarkar, "A bi-stage feature selection approach for COVID-19 prediction using chest CT images," *Appl. Intell.*, vol. 51, pp. 8985–9000, 2021.
- [49] R. R. Selvaraju, M. Cogswell, A. Das, R. Vedantam, D. Parikh, and D. Batra, "Grad-CAM: Visual explanations from deep networks via gradient-based localization," in *Proc. IEEE Int. Conf. Comput. Vis.*, 2017, pp. 618–626.
- [50] X. Ding, J. Xu, J. Zhou, and Q. Long, "Chest CT findings of COVID-19 pneumonia by duration of symptoms," *Eur. J. Radiol.*, vol. 127, 2020, Art. no. 109009.
- [51] F. Pan et al., "Time course of lung changes at chest CT during recovery from coronavirus disease 2019 (COVID-19)," *Radiol.*, vol. 295, no. 3, pp. 715–721, 2020.
- [52] R. M. M. Ali and M. B. I. Ghonimy, "Radiological findings spectrum of asymptomatic coronavirus (COVID-19) patients," *Egyptian J. Radiol. Nucl. Med.*, vol. 51, no. 1, pp. 1–6, 2020.
- [53] H. Meng et al., "CT imaging and clinical course of asymptomatic cases with COVID-19 pneumonia at admission in Wuhan, China," *J. Infection*, vol. 81, no. 1, pp. e33–e39, 2020.